Spatial noise correlations beyond nearest neighbors in math xmlns="http://www.w3.org/1998/Math/MathML" display="inline" overflow="scroll">msup>mi>/mi>mn>28/mn>/msup>mi>Si/mi>mo>//mo>/math>Si-Ge spin qubits

J.S. Rojas-Arias, A. Noiri, P. Stano, T. Nakajima, J. Yoneda, K. Takeda, T. Kobayashi, A. Sammak, G. Scappucci, D. Loss, and S. Tarucha

Spatial noise correlations beyond nearest-neighbor in ^{28}Si/SiGe spin qubits

J. S. Rojas-Arias,[1, *] A. Noiri,[2] P. Stano,[2, 3] T. Nakajima,[2] J. Yoneda,[4] K. Takeda,[2]
T. Kobayashi,[1] A. Sammak,[5] G. Scappucci,[6] D. Loss,[2, 1, 7] and S. Tarucha[2, 1, †]

[1] *RIKEN, Center for Quantum Computing (RQC), Wako-shi, Saitama 351-0198, Japan*
[2] *RIKEN, Center for Emergent Matter Science (CEMS), Wako-shi, Saitama 351-0198, Japan*
[3] *Slovak Academy of Sciences, Institute of Physics, 845 11 Bratislava, Slovakia*
[4] *Tokyo Institute of Technology, Tokyo Tech Academy for Super Smart Society, Tokyo 152-8552, Japan*
[5] *QuTech and Netherlands Organisation for Applied Scientific Research (TNO), Stieltjesweg 1, 2628 CK Delft, Netherlands*
[6] *QuTech and Kavli Institute of Nanoscience, Delft University of Technology, Lorentzweg 1, 2628 CJ Delft, Netherlands*
[7] *Department of Physics, University of Basel, Klingelbergstrasse 82, CH-4056 Basel, Switzerland*

We detect correlations in qubit-energy fluctuations of non-neighboring qubits defined in isotopically purified Si/SiGe quantum dots. At low frequencies (where the noise is strongest), the correlation coefficient reaches 10% for a next-nearest-neighbor qubit-pair separated by 200 nm. Correlations with the charge sensor signal reach up to 70%, proving that the observed noise is of electrical origin. A simple theoretical model quantitatively reproduces the measurements and predicts a polynomial decay of correlations with interqubit distance. Our results quantify long-range correlations of noise in quantum-dot spin-qubit arrays, essential for their scalability and fault-tolerance.

I. INTRODUCTION

Noise is an obstacle for the realization of quantum computing. Qubits are coupled to noisy environments that perturb the whole computational sequence: initialization, manipulation, evolution and readout. While progress in improving each of these stages is notable [1–18], decreasing noise further is a challenging task that requires understanding of the noise origin and properties. The required level of understanding grows as the noise is pushed to smaller magnitudes. In addition, none of the pursued computational platforms, including semiconductors, will become noise-free. The need for quantum error correction (QEC) will thus remain. However, the error thresholds and even the feasibility of a given QEC scheme depend on the noise type. Correlations of the noise in space (across different qubits) can be especially detrimental [19–26]. Such inter-qubit noise correlations have been observed recently for semiconductor qubits in Ref. [27].

In spin qubits defined by trapping individual electrons in semiconductor quantum dots (QDs) [28, 29], the coherence time is limited by magnetic and electric noise. The most relevant source of magnetic noise is the collective Overhauser field from nuclear spins of the host material, coupled to the qubit via the hyperfine interaction [30–33]. The shift to materials which have zero-spin isotopes, such as silicon, has led to a significant improvement on coherence times [34–36]. While isotope purification improves coherence further [7, 18, 37, 38], the residual nuclear spins can still be the dominant decoherence source [10, 39–42]. On the other hand, electrical noise (charge noise) [43] couples to a spin qubit via spin-orbit interactions. In materials without a sizable intrinsic spin-orbit coupling, electric control of the

spin requires to implement an extrinsic one, using micro magnets [44–46]. Thus, irrespective of the material and its level of isotopic purification, the first question concerning the noise observed in a current-generation semiconducting device is whether it is dominated by magnetic or electric fluctuations.

The first step in analyzing noise is to inspect its spectrum. Being physically very different, one hopes that magnetic and electric noise will have distinct spectra: the ubiquitous $1/f$-like spectra [47] suggest charge noise [48] while $1/f^2$ high-frequency tail suggests nuclei [49, 50]. Unfortunately, this rule of thumb is not reliable. In experiments, the charge noise powers range from small to large ($1/f^{0.65}$ in Ref. [51] versus $1/f^2$ in Ref. [37]), show large differences between similar devices [52], and for a given device are different in different frequency ranges [53]. The analysis is further impeded by the lack of consensus on the origin of charge noise [54, 55] and by the lack of knowledge of the microscopic details of the quantum dot environment: the spectrum of the nuclear-spin noise is not a simple power law [31] and its exact shape depends on the nuclear spin diffusion, in turn depending on those microscopic details. For example, the subdiffusive behavior of the Overhauser field observed in Refs. [56, 57] remains unexplained.

One of the major findings of this article is that the noise nature (it is charge noise in our device) can be ascertained from spatial correlations, both qubit-qubit and qubit-sensor ones. We demonstrate it on a three quantum-dot device made in ^{28}Si/SiGe heterostructure, where we quantify spatio-temporal correlations of dephasing noise affecting the outer two quantum dots. The two dots are approximately 200 nm apart but, more importantly, they are not the nearest-neighbors in the array. Despite this physical separation, we find clear spatial correlations of the energy fluctuations of the spin qubits hosted in the two dots. Based on the correlations, we conclude that the underlying noise is charge

* juan.rojasarias@riken.jp
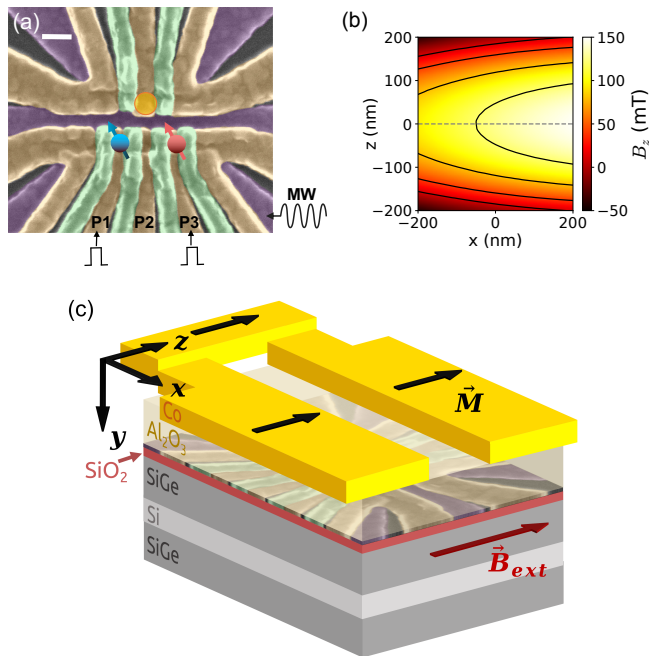† tarucha@riken.jp

FIG. 1. (a) A false color scanning electron microscope image of a device nominally identical to the one measured. The white scale bar indicates 100 nm. (b) The simulation of the z component of the micro-magnet field in the QD plane. (c) A schematic depiction of the structure layers with the micro-magnet (yellow) on top and a thin SiO₂ layer (red) right below the metallic gates.

noise originating in the device. We also devise a microscopic model interpreting the noise as an ensemble of two-level charge fluctuators localized nearby the quantum dot array. The model quantitatively agrees with the measurement results and allows us to estimate the expected variability of noise spectra and the scaling of correlations with qubit-qubit separation in similar devices.

The paper is organized as follows: In Sec. II, we describe the device. In Sec. III, we outline the measurement protocol and show the noise spectra including spatial correlations. In Sec. IV, we analyze the noise origin from the qubit-charge sensor correlations. In Sec. V, we discuss the dephasing mechanism and our model of the observed noise spectra. We summarize in Sec. VI.

II. SILICON TRIPLE QUANTUM DOT DEVICE

The triple quantum dot (TQD) device shown in Fig. 1a was fabricated by patterning of overlapping aluminium gates [58] on top of an isotopically purified ²⁸Si/SiGe wafer (800 ppm ²⁹Si). The wafer is composed of a 10 nm thick Si quantum well, a 50 nm SiGe spacer, and a 2 nm SiO₂ cap. The gates consist of screening (purple in Fig. 1a), accumulation (orange), and barrier

(green) gates, with a thickness of 25 nm, 45 nm and 65 nm, respectively. We tune the device to the (1,0,1) charge configuration, meaning that single electrons are trapped in the left- and right-most dots (blue and red arrows in Fig. 1a, respectively), underneath the plunger gates P1 and P3, which are separated by 180 nm. The middle dot remains empty throughout the experiment. Qubits are defined in the spin states of the electrons, Zeeman-split by the applied in-plane external magnetic field $B_{ext} = 0.45$ T. With a sensor QD (orange circle in Fig. 1a) in the vicinity of the TQD structure, we read out the spin states by spin-to-charge conversion via energy selective tunneling [59], which is also used for initialization. Fast single-shot spin readout is achieved by radio-frequency reflectometry by coupling the sensor QD to a tank circuit [13].

Electric control of the spin qubits is executed via electric-dipole spin resonance. It is enabled by a magnetic field gradient of a micro-magnet [45] located on top of the device. It is insulated from the metallic electrodes (Fig. 1c) with a 30 nm thick aluminium oxide layer grown by atomic layer deposition. A simulation of the micro-magnet magnetic field parallel to the externally applied field is presented in Fig. 1b. For the simulation, we employed the COMSOL Multipyshics® software with a 3D geometry following the fabrication parameters of our layered structure, including a simplified geometry for the overlapping aluminium gates. The qubit Rabi frequencies are $f_L^{Rabi} = 3.73$ MHz and $f_R^{Rabi} = 4.07$ MHz, with the subscript L (R) referring to the left (right) qubit. The measured coherence times are $T_{2,L}^* = 6.1$ μs and $T_{2,R}^* = 6.9$ μs for an integration time of 100 seconds. Because the typical qubit energy fluctuations are much larger than the measured remnant exchange coupling, $J = 0.9$ kHz [60], the qubits can be considered non-interacting.

III. QUBIT-FREQUENCY AUTO AND CROSS CORRELATIONS

In our work, we study dephasing noise manifested as fluctuations in the resonant energy of the qubits. In order to probe the spatio-temporal correlations, we measure interleaved Ramsey oscillations of the qubits repeatedly and estimate the time evolutions of their resonant energies using a Bayesian algorithm [56]. An interleaved Ramsey cycle starts with the initialization of the two qubits to the spin down state. Next, a $\pi/2$ pulse, a free evolution time t_e, and a second $\pi/2$ pulse are applied to qubit L, followed by the same sequence applied to qubit R. The cycle is finalized by readout of the spin state of both qubits. Each cycle takes 2.09 ms and is repeated for t_e increasing from 0.04 μs to 4 μs, in 0.04 μs steps. This repetition of cycles forms a record. An energy value for each qubit is extracted from a single record by Bayesian estimation [56, 57]. Collecting data from 10^5 records, we obtain the time evolution of the qubit energies covering a time span of 5 hours 48

minutes. Two typical samples of the time evolution are plotted as insets in Fig. 2a. One can see fast fluctuations modulated by a slow switching between two discrete levels in both qubits, each of them with different rates. The switching in one qubit appears to be independent from the other at first sight, but we will make the statement more precise below.

To analyze the spectral content of the noise, we define the following power spectrum,

$$C_{\alpha\beta}(f) = \int_{-\infty}^{\infty} d\tau e^{2\pi i f \tau} \langle \delta\nu_\alpha(t)\delta\nu_\beta(t+\tau)\rangle. \quad (1)$$

Here, τ is the time delay of two signals $\delta\nu_\alpha$ and $\delta\nu_\beta$, that in our case are qubit energy fluctuations measured with respect to an arbitrary reference value. The indexes label qubits $\alpha, \beta \in \{L, R\}$, and $\langle\cdots\rangle$ denotes a statistical average over time t. For equal indexes, $\alpha = \beta$, the general formula yields the auto power spectral density (auto-PSD), $S_\alpha \equiv C_{\alpha\alpha}$. It is a real and symmetric function of the frequency f and gives the frequency spectrum of the signal $\delta\nu_\alpha$. On the other hand, the cross power spectral density (cross-PSD) $C_{LR} = C_{RL}^*$ is, in general, complex and gives frequency-resolved correlation between the two signals and, in turn, the spatial correlations of the noise.

It is common to relate the auto-PSDs and the cross-PSD introducing the normalized cross-PSD, also known as the correlation coefficient:

$$r(f) = \frac{C_{LR}(f)}{\sqrt{S_L(f)S_R(f)}}. \quad (2)$$

The normalized cross-PSD is a complex function $r(f) = |r(f)|e^{i\phi(f)}$. Its magnitude measures the proportion of correlated noise with respect to the total noise and its phase describes the correlations type: At a given frequency, $|r| = 1$ corresponds to perfect spatial correlations while $|r| = 0$ means independent (uncorrelated) noise. With a finite $|r|$, $\phi = 0$ corresponds to positive correlations, $\phi = \pi$ to negative correlations (anticorrelations), and other values can be interpreted as a time lag between the two signals.

We evaluated the auto-PSD for each qubit using the methods of Ref. [61], which deliver not only the estimated values of the PSDs but also the confidence level of the estimations. The results are plotted in Fig. 2a and show a Lorentzian ($\propto f^{-2}$) dependence at frequencies lower than 0.01 Hz in both qubits. A Lorentzian spectrum arises if the qubit is coupled to a randomly switching two-level system (TLS) [62]. The corresponding qubit-energy switches can be seen in the time traces. The normalized cross-PSD (Figures 2b and 2c) in this frequency range shows positive correlations with a magnitude between 0 and 0.3. However, the level of confidence (represented as a color gradient) is too low for a definite judgement about finite correlations [63]. We conclude that, most probably, the low-frequency noise is dominated by each qubit being coupled to its own TLS, the two being independent. The TLSs are either charge
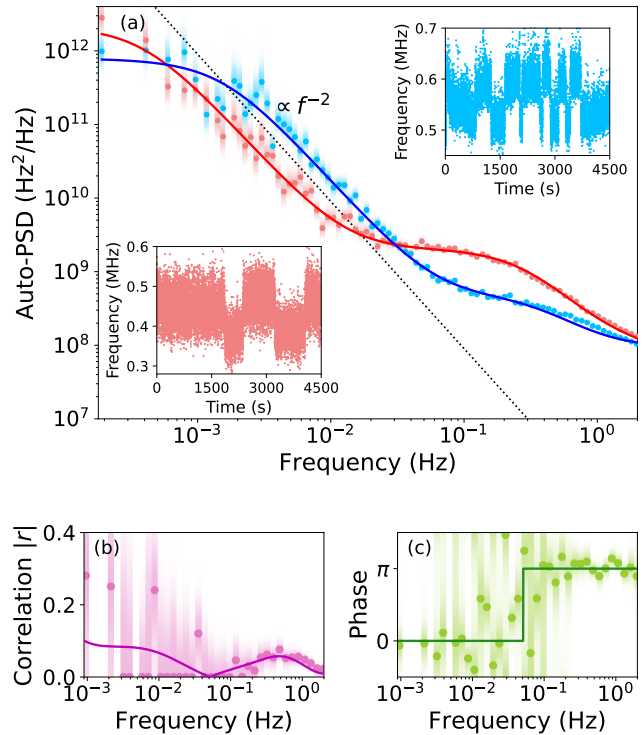

FIG. 2. (a) The power spectral density of the left (blue) and right (red) qubit-energy fluctuations. The dotted line corresponds to a f^{-2} dependence as a reference. Inset: sample time traces of each qubit energy showing a 2-level switching behavior; the color code follows that of the main panel. (b-c) The correlation coefficient amplitude (b) and phase (c). In all panels, the color gradient represents the estimating distribution of the corresponding quantity at each frequency with the maximum likelihood estimator marked as points (details are discussed in Ref. [61]); the continuous lines are calculated from the TLSs set given in Fig. 4.

defects (charge traps or dipolar fluctuators; see below) with long (>1000 s) switching times [43, 64], or it could be single nuclear spins hyperfine coupled the qubits [42].

The higher-frequency parts of the auto-spectra exhibit different slopes for each qubit and their relation with the time-traces is not straightforward. Nevertheless, the normalized cross-PSD displays two interesting features in this regime. First, despite the large separation between qubits, spatial noise correlations reach up to $|r| \sim 0.1$ (around 0.4 Hz). Second, these finite correlations have a well-defined phase. At higher frequencies, the phase is π, while there seems to be a transition to phase 0 around 0.06 Hz. The well-defined phase further confirms that the correlations are beyond coincidence: within the range 0.1–1 Hz, the fluctuations in the resonant energies of the two qubits are correlated.

After presenting the data, we next discuss the noise origin and propose a simple microscopic model for it.

IV. IDENTIFYING THE ORIGIN OF THE NOISE

Our a priori expectation concerning the noise in the device is that it is either charge noise or magnetic noise due to the remnant ^{29}Si. As explained in the introduction, it is difficult to infer the noise origin from the auto power spectra. In this section, we discuss the qubit-qubit cross-correlations as more revealing concerning the noise source [27] and reason that they suggest that charge noise dominates. We demonstrate this dominance unequivocally by detecting high cross-correlation between the fluctuations of the qubit energies and the charge sensor voltage shifts.

Let us start with qualitative estimates. Given the typical size of our QDs ($\approx$ 28 nm in diameter for a 2 meV harmonic confinement), the maximum hyperfine coupling strength achievable for a single nuclear spin is about 10 kHz [calculated with Eq. (A1)], about one order of magnitude smaller than the two-level frequency switching seen in the time-traces in Fig. 2a. Similarly for the auto-correlation spectra: In App. A, we estimate the auto-PSD due to diffusive nuclear spins and find that it is at least an order of magnitude too low to account for the auto-PSD at any frequency. When we apply the same model to cross-correlations, the discrepancy becomes much more drastic: The calculation predicts cross-correlations due to nuclei that are orders of magnitude lower than the measured values. In other words, magnetic noise is expected to be highly local. This fact is the consequence of the negligible overlap of the electron wave functions in the non-neighboring dots. On the other hand, it is natural to expect non-local correlations in charge noise involving long-range Coulomb interactions. We conclude that these are hints that nuclear spin noise does not play a significant role in the low-frequency noise of our device. This conclusion would be in line with previous work on isotopically purified silicon devices with a micro-magnet [7]. On the other hand, these are hints only, since it is hard to exclude a possibility of some correlated nuclear dynamical polarization effects, or non-local nuclear spin flip-flops, or similar.

To conclusively determine that our device is dominated by charge noise, we now analyze the cross-PSD between the qubit energies and the charge sensor signal. We define a single-shot readout voltage value as the difference between the highest and the lowest voltages measured during the readout window from the radio-frequency reflectometry setup [13]. Then, we define the charge sensor signals V_L^σ and V_R^σ as the average of all the single-shot voltage outcomes with the same spin-state readout $\sigma \in \{\uparrow, \downarrow\}$, taken from a record obtained while measuring the left and right qubit, respectively. In this way, following our energy-selective-tunneling measurement scheme, V_L^σ refers to the charge sensor signals taken at a point in the transition line between charge states $(1,0,1) \leftrightarrow (0,0,1)$. Similarly, V_R^σ are the signals at a point belonging to the $(1,0,1) \leftrightarrow (1,0,0)$ transi-
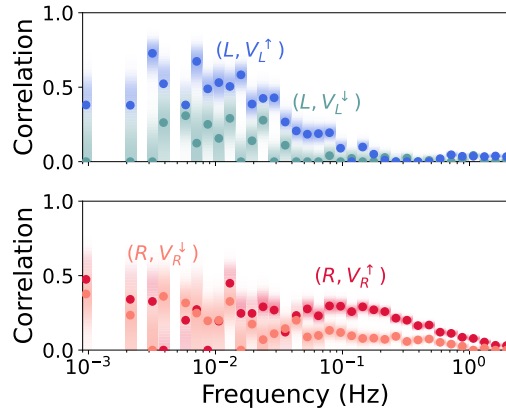

FIG. 3. Normalized cross-PSD between the qubit energies and the charge sensor signals $V_L^{\uparrow,\downarrow}$ and $V_R^{\uparrow,\downarrow}$. The upper (bottom) panel shows the correlations for the left (right) qubit. Similar to Fig. 2, the color gradients represent the probability distribution of the cross-PSD, with the maximum marked with circles. The corresponding phases and auto-PSDs are presented in Appendix B.

tion line. The voltages $V_\alpha^\uparrow$ correspond to measurements with the presence of a 'blip' in the charge sensor signal, indicating the occurrence of an electron-tunneling event, whereas $V_\alpha^\downarrow$ correspond to measurements in the absence of electron tunneling to the reservoir [59]. As such, $V_\alpha^\downarrow$ contain information of the charge configuration $(1,0,1)$ whereas $V_\alpha^\uparrow$ contain information of not only the $(1,0,1)$ charge state but also the "non-qubit" configurations: $(0,0,1)$ for $\alpha = L$ and $(1,0,0)$ for $\alpha = R$ (for the exact definitions, see Appendix B) [65]. Figure 3 shows the normalized cross-PSD amplitudes between the qubit energies and the charge sensor signals, obtained from Eq. (1) using V_α^σ as one of the signals. There are correlations as high as ~ 0.7 for the left qubit and ~ 0.5 for the right one. These strong correlations with the signal of the charge-sensor (assumed largely insensitive to magnetic noise) are firm evidence of charge noise being dominant in our device.

We point out that the evaluation of the correlations between the qubit energy and the charge sensor signal does not require additional measurements. We obtained them from the Ramsey data used to plot Fig. 2. Therefore, *such correlations can be extracted even from previously reported single-qubit experiments.* With this method, if strong correlations are found it is possible to directly determine whether a device is (was) dominated by electric noise, instead of relying on the analysis of auto-spectra [7, 37]. Having confirmed that charge noise is the dominant dephasing mechanism here, in what follows we see how it can account for the measured noise spectra quantitatively.

V. NOISE MODEL: AN ENSEMBLE OF CHARGE FLUCTUATORS

Perhaps the most popular model to account for $1/f$-like spectrum is to consider a superposition of Lorentzian spectra, an idea that goes back to Bernamont [66]. An ensemble of TLSs, each of which has a Lorentzian spectrum [67], can have the suitable distribution of switching times under plausible assumptions [68–70]. In a solid-state device, such TLSs are expected to be present due to fabrication imperfections or inherent crystal defects. While their location and nature remain unclear [54], the amorphous oxide (colored red in Fig. 1c), and the semiconductor/oxide interface are probable hosts [55].

We follow this idea and relate the observed noise to a TLS ensemble. While such modeling is not new [35, 52, 71], we point out two differences to previous works. First, we do not fit the spectra that we observe to $1/f$-like power laws, in turn invoking a large (in the limit, infinite) ensemble of TLSs. We find it hard to reconcile the idea of an infinite number of TLSs with our nanometer-sized dots and the non-uniform spectral features that we observe. Second, we fit the whole set of spectral data shown in Fig. 2, including the auto-PSD of both qubits, and the cross-PSD magnitude and phase, to a single set of TLSs. Surprisingly, we find that a collection of a few TLSs located around the quantum dot array can reproduce quantitatively all observed qubit noise features, including the intricate dependence of the normalized cross-PSD magnitude and the correlation-anticorrelation crossover in its phase.

A. A few TLSs as the charge noise source

We assume that the noise in the qubit energies arises due to fluctuating electric fields. We denote the field at the location of the dot α as $\delta \vec{E}_\alpha$ and assume that it is constant over the single-dot lateral dimensions. The field affects the qubit by shifting the dot center, which, due to the non-uniform micro-magnet field (see Fig. 1b), changes the spin-qubit energy by $\delta\nu_\alpha$. Assuming parabolic lateral confinement, we have

$$\delta\nu_\alpha = \frac{g\mu_B}{2\pi\hbar}\frac{e}{m\omega_\alpha^2}\left(\frac{\partial B_\alpha}{\partial x}\delta E_\alpha^x + \frac{\partial B_\alpha}{\partial z}\delta E_\alpha^z\right), \quad (3)$$

where $\hbar\omega_\alpha$ is the confinement energy, B_α is the z component of the magnetic field at QD α location, μ_B is Bohr's magneton, e is the electron charge, m is the effective mass, and g is the g-factor. We neglect the QD shifts along the growth direction where the confinement is stronger.

We assign the fluctuating electric fields from Eq. (3) to charge fluctuations δq_i of an ensemble of TLSs,

$$\delta\vec{E}_\alpha = \sum_i \frac{1}{4\pi\epsilon\epsilon_0}\frac{\vec{x}_\alpha - \vec{x}_i}{|\vec{x}_\alpha - \vec{x}_i|^3}\delta q_i. \quad (4)$$
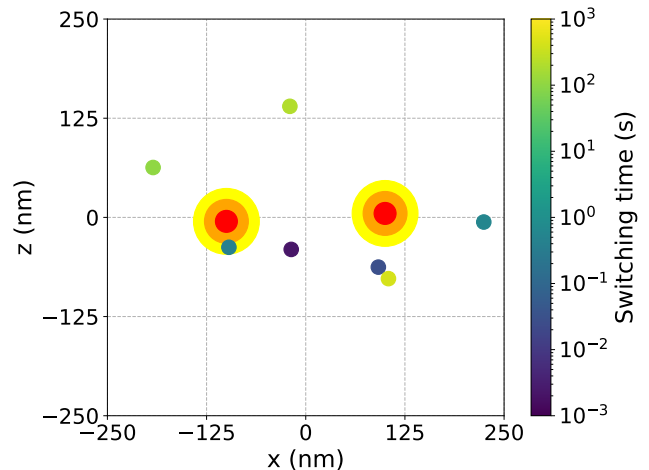

FIG. 4. One possible set of TLSs that reproduces the experimental data. The tonality gives the switching time of the corresponding TLS. All TLSs are located 50 nm above the QD plane and have an opposite image charge 4 nm further above. The two disks in the center correspond to the QDs with yellow, orange, and red representing 3, 2, and 1 standard deviations of the electron's probability distribution, respectively, for a 2 meV parabolic confinement. The QDs are located at $(x, z) = (\pm 100 \text{ nm}, \pm 5 \text{ nm})$. We used $m = 0.2\, m_0$ with m_0 the free electron mass and $\epsilon = 13$.

Here, i is the TLS label, ϵ is the effective dielectric constant of the layered structure, ϵ_0 is the permittivity of vacuum, $\vec{x}_\alpha$ is the QD center, and $\vec{x}_i$ the TLS position. We assume that TLSs are independent, their charge state switches between empty $\delta q_i = 0$ and occupied $\delta q_i = \pm e$, with a characteristic switching time t_i. These properties are grasped by the correlator

$$\langle\delta q_i(t)\delta q_j(t+\tau)\rangle = \frac{e^2}{4}\left[1 + \delta_{ij}\exp(-\tau/t_i)\right]. \quad (5)$$

Given a distribution of TLSs and the location of the QDs, Eqs. (1), (3), (4), and (5) allow us to calculate the auto-PSDs and the cross-PSD, from which we obtain the correlation coefficient using Eq. (2).

We use a least squares minimization algorithm to fit the correlation spectra. We increase the number of TLSs until a satisfactory fit is realized, with the lateral coordinates (x and z) and the switching time of every TLS as the fitting parameters. Importantly, we include image charges, $-\delta q_i$, putting one above every TLS. In this way, in the model we approximate the screening due to structure metals [72] by screening from a metallic plane (placed above the oxide, at $y = -52$ nm; the QD plane is at $y = 0$ nm). The rest of the parameters are fixed as follows. We set all TLSs to $y = -50$ nm, being the interface between the SiGe spacer and the SiO$_2$ layer. Concerning the effects on a single qubit, the TLS shift along y farther (closer) to the screening plane can be compensated by a shift closer to (away from) the qubit laterally. While the in-oxide depth of a TLS might be correlated to its switching time [73], in our model we
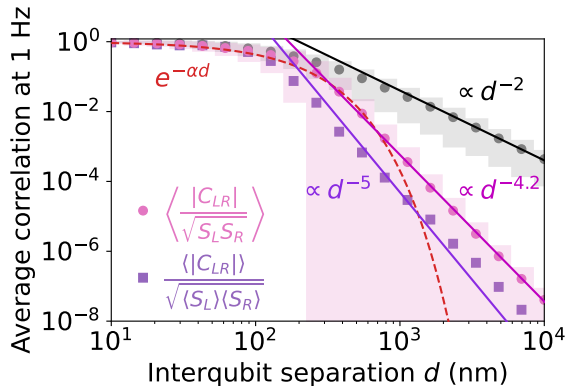
FIG. 5. Average normalized correlation amplitude at 1 Hz as a function of the interqubit separation. Pink (gray) circles correspond to the simulation of $\langle r \rangle$ with (without) screening due to the metallic gates. Shaded regions represent one standard deviation. Purple squares correspond to $\bar{r}$. For reference, the red dotted line corresponds to an exponential decay $\exp(-\alpha d)$ with $\alpha = 0.0085$ nm^{-1}, while the magenta (black) curve is proportional to $d^{-4.2}$ (d^{-2}). The purple line is $\propto d^{-5}$ following the result from Appendix D.

do not consider such a link and keep switching times as independent parameters. The best achievable fit would then not be substantially improved by allowing for small additional variations of the y coordinate of the TLSs. We also limit ourselves to one image charge per TLS, even though the model could be extended to include more images to account for higher order effects at the interfaces between dielectrics. The values of the magnetic field gradients follow from Fig. 1b and the QD locations. Although we do not precisely know the latter, the measured anti-correlations suggest that the qubits could be subject to opposite magnetic gradients. Therefore, as an example, we slightly displace the two dots asymmetrically along the z axis.

Figure 4 depicts one set of TLSs that leads to the curves in Fig. 2. The spectral content of the noise and the type and strength of correlations are quantitatively accounted for by the model with only seven TLSs, corresponding to a density $n_c \sim 10^{10}$ cm^{-2}. We point out the significance of screening when obtaining this value, in line with Ref. [74]; if we remove the image charges from the model, the noise from even a single TLS in the vicinity of the dots is already about two orders of magnitude larger than the measured auto-PSDs.

B. Scaling of noise correlations with distance

Perhaps more crucial than the magnitude of the noise correlations is their scaling with interqubit separation [19, 20]. We take advantage of our model to investigate this scaling by simulation of qubits with increasing separation. For these simulations we locate the qubits at $(x, z) = (\pm d/2, 0)$ and assign fixed magnetic gradients $\partial B/\partial x = 0.1$ mT/nm and $\partial B/\partial z = 0$ for both

qubits, irrespective of their separation d. We generate 3000 random distributions of TLSs in a square-shaped area of 35 μm side length, with switching times in the range $(10^{-5}, 10^5)$ s, using linearly and logarithmically uniform distributions for space and time, respectively [75]. In these simulations, we keep the remaining parameters the same as in Sec. V A, including the TLS density $n_c = 10^{10}$ cm^{-2}. Since each distribution yields different spectral characteristics (see Appendix C) and the PSDs are not self-averaging [76], we characterize the generated ensemble by both the average and the standard deviation at each frequency. We evaluate two quantities: the average normalized cross-PSD magnitude $\langle r \rangle \equiv \langle |C_{LR}|/\sqrt{S_L S_R} \rangle$, and the average cross-PSD magnitude normalized by the average auto-PSDs $\bar{r} \equiv \langle |C_{LR}| \rangle / \sqrt{\langle S_L \rangle \langle S_R \rangle}$, introduced for comparison with analytic results. We plot these quantities at 1 Hz as a function of the qubit separation in Fig. 5. The average correlation $\langle r \rangle$ initially appears to decay exponentially, but eventually a polynomial tail $\propto d^{-4.2}$ is observed at large interqubit separations. While we observe that $\bar{r}$ is smaller than $\langle r \rangle$, a similar polynomial tail appears. To highlight the effect of screening, we perform the same simulation without the image charges and obtain the gray circles, which show a much slower decay $\langle r \rangle \propto d^{-2}$. We note that these averages calculated from random sampling show a trend but may require large ensembles to ensure convergence. To confirm the observed trends, we turn to an analytic result, which can be obtained for $\bar{r}$. The derivation is presented in Appendix D and yields $\bar{r} \propto d^{-5} + \mathcal{O}(d^{-7})$, shown as a purple curve in Fig. 5. Given the similar polynomial decays in simulations, we conjecture that $\langle r \rangle$ also follows the $\propto d^{-5}$ decay in the limit $d \to \infty$ (we could not obtain analytic results for it). In any case, given the power-law decay of spatial correlations, screening becomes essential for such correlations to decay fast enough to enable error correction [77].

C. Implications of a-few-TLS model

We mention a few things that can be learned from these investigations. First, charge noise properties reflect a specific distribution of TLSs which is device—and potentially also cooldown—dependent. Unless these sources reach some kind of self-averaging statistical limit, a single set of PSDs from a given device will not fit any generic theory predicting universal behavior. Second, the distribution of TLSs leading to particular spectral characteristics is not unique (see Appendix E). Third, while each TLS affects both qubits and individually induces perfectly correlated noise, spatial correlations will decrease upon adding noise from a collection of fluctuators with different couplings [25]. This, perhaps counter-intuitive, behavior is shown in Fig. 10, where a high density of TLSs suppresses the degree of noise correlation between qubits. Fourth, while we considered charge traps in the oxide, defects in the quantum well

[78] could contribute as well. In this case, we point out again that they should be of dipolar nature, since an unscreened charge trap would cause a noise magnitude inconsistent with our measurements. Nevertheless, as explained in Sec. V A, our main results, especially the scaling with distance, remain unaltered: A charge trap close to a screening plane is equivalent to a fluctuating charge dipole. Finally, screening plays a major role in both the magnitude and range of the noise. A high density of metallic gates close to the substrate surface screening TLSs seems beneficial, favoring overlapping gate designs such as the one used here. Even though we measured correlated noise beyond nearest-neighbor qubits, screening makes spatial correlations decay fast enough such that QEC remains feasible.

VI. CONCLUSIONS

We measured the auto- and cross-correlation noise spectra of non-neighboring spin qubits defined in ^{28}Si/SiGe quantum dots. Our main result is observing clear cross-correlations in the frequency range 0.1–1 Hz, with a magnitude about 10%, despite the qubits being non-neighboring. In addition, we found strong correlations ($\sim 70\%$) between the qubit energies and the charge sensor signal, providing indisputable evidence that charge noise is the dominant dephasing mechanism in our qubits. We were able to quantitatively reproduce the measured data by modeling the noise as a superposition of a few independent charge two-level systems located in an oxide layer of the device. Our model explains the variability in charge noise spectra across nominally identical devices and highlights the importance of screening not just to decrease the noise magnitude but also its range. We predict a polynomial decay of noise cross-correlations with interqubit separation which could be checked in future measurements in larger spin qubit arrays. Our study motivates further research on noise spatial correlations, not only in spin qubit systems but in any candidate for quantum computing. Noise correlation properties are crucial for the implementation of quantum error correction and are another important benchmark to take into account.

ACKNOWLEDGMENTS

Appendix A: Spatial correlations due to nuclear spin noise

Here we reason that the nuclear spins cannot cause the observed correlations. We do so by calculating the auto- and cross-PSD via a model of diffusive nuclei following Refs. [30–32, 79]. The energy shift $\delta\nu$ of a qubit with spin $\vec{S}$ due to nuclear spins $\vec{I}_n$ is

$$\delta\nu = \frac{v_0 A}{2\pi\hbar} \sum_n |\psi(\vec{x}_n)|^2 I_n^z, \tag{A1}$$

where $\psi(\vec{x})$ is the electron's wave function, v_0 the unit cell volume and $A = 2.4$ μeV the hyperfine coupling strength for ^{29}Si [80–82]. We replace the discrete summation over nuclei by an integral over space introducing the (dimensionless) nuclear polarization density $P(\vec{x}, t)$:

$$\delta\nu = \frac{pA}{2\pi\hbar} \int d^3x \ P(\vec{x}, t)|\psi(\vec{x})|^2,$$

with p the fraction of ^{29}Si nuclei.

The dynamics of the nuclei with their magnetic dipole-dipole interaction show a diffusion-like behavior in the absence of nuclear spin relaxation. Thus, we write the evolution of the nuclear polarization as:

$$\frac{\partial P(\vec{x}, t)}{\partial t} = D\nabla^2 P(\vec{x}, t).$$

The stochastic nature of the nuclear spins is grasped by inserting a stochastic force $\xi(\vec{x}, t)$ into the diffusion equation for P. Moving to Fourier space this leads to:

$$\frac{\partial P_{\vec{k}}(t)}{\partial t} = -4\pi^2 k^2 D P_{\vec{k}}(t) + \xi_{\vec{k}}(t).$$

Solving the diffusion equation we obtain for an unpolarized system:

$$P_{\vec{k}}(t) = \int_0^\infty dt' \ \xi_{\vec{k}}(t - t')e^{-4\pi^2 k^2 D t'}. \tag{A2}$$

Now, we are interested in calculating the cross-correlator $C_{LR}(t, t') \equiv \langle \delta\nu_L(t)\delta\nu_R(t') \rangle$. To do so, we assume that the statistics of the random forces are independent in space and time:

$$\langle \xi_{\vec{k}_1}(t_1)\xi_{\vec{k}_2}(t_2) \rangle = \delta(t_1 - t_2)\delta(\vec{k}_1 + \vec{k}_2)\Xi(k_1). \tag{A3}$$

From Eqs. (A2) and (A3) we get the following cross-correlator:

$$\begin{aligned} C_{LR}(t, t') = {} & pA^2 \frac{I(I + 1)}{3} v_0 \\ & \times \int d^3k \ |\psi_L|^2_{\vec{k}} |\psi_R|^2_{-\vec{k}} \ e^{-4\pi^2 k^2 D|t - t'|}, \end{aligned} \tag{A4}$$
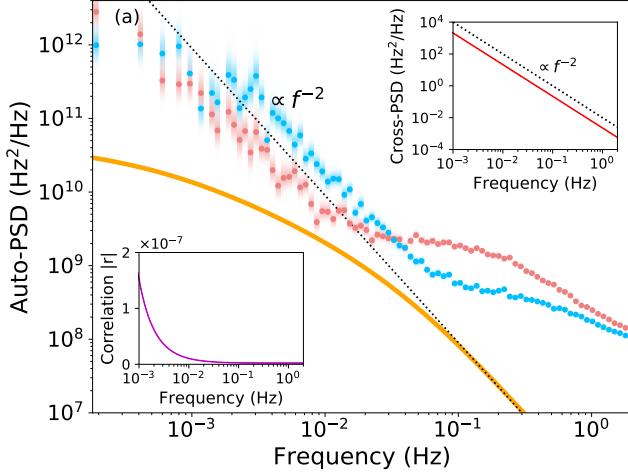
FIG. 6. The main panel of Fig. 2a including the auto power spectral density of the nuclear spin noise (orange) calculated according to Eq. A5 for $d = 0$. Insets: cross power spectral density and correlation coefficient calculated for an interdot separation of 200 nm. The dotted lines are for reference.

where we evaluated $\Xi(k) = 8\pi^2 k^2 DI(I+1)v_0 p/3$ by direct calculation of $C_{LL}(t,t)$ from Eq. (A1). The cross correlator from Eq. (A4) can be evaluated if we assume a Gaussian form for the electron wavefunction:

$$|\psi_\alpha(\vec{x})|^2 = \frac{1}{\pi^{3/2}l_p^2 l_y} \exp\left(-\frac{(x-x_\alpha)^2 + z^2}{l_p^2} - \frac{y^2}{l_y^2}\right),$$

with l_p and l_y the spreads in-plane and out-of-plane, respectively. Using this we get the final result for the cross-correlator:

$$C_{LR}(t,t') = \frac{C_0 \exp[-\kappa/(1+\gamma|t-t'|)]}{(1+\gamma|t-t'|)(1+\gamma\zeta|t-t'|)^{1/2}}, \quad (A5)$$

where we defined $\gamma = 2D/l_p^2$, $\kappa = 2d^2/l_p^2$, $\zeta = l_p^2/l_y^2$, $2d = x_R - x_L$ and:

$$C_0 = p\frac{A^2}{\sqrt{2\pi}}\frac{I(I+1)}{3}\frac{a_0^3}{8V_D}, \quad (A6)$$

with a_0 the lattice constant of silicon and $V_D = 2\pi l_p^2 l_y$ the QD volume. The Fourier transform of Eq. (A5) gives us the cross-PSD from which we can evaluate the spatial correlations. The auto-PSD is obtained by setting $d = 0$ and it is plotted in Fig. 6 for $D = 0.4 \text{ nm}^2/\text{s}$ [83] and a typical QD size of $(l_p, l_y) = (14 \text{ nm}, 3 \text{ nm})$. There we can see that the nuclear noise auto-PSD is lower than the measured values, giving further indication that the main dephasing mechanism is charge noise. The correlation coefficient is $|r| < 10^{-6}$ in the frequency range of interest as shown in the insets of Fig. 6, a value much smaller than that displayed in Fig. 2b. This very small value occurs because the Overhauser field experienced by the qubits is determined by the spread of their respective wave function; if there is not a considerable overlap, the local nuclear dynamics evolve independently. Thus, nuclear spin noise is uncorrelated at appreciable interdot separations.
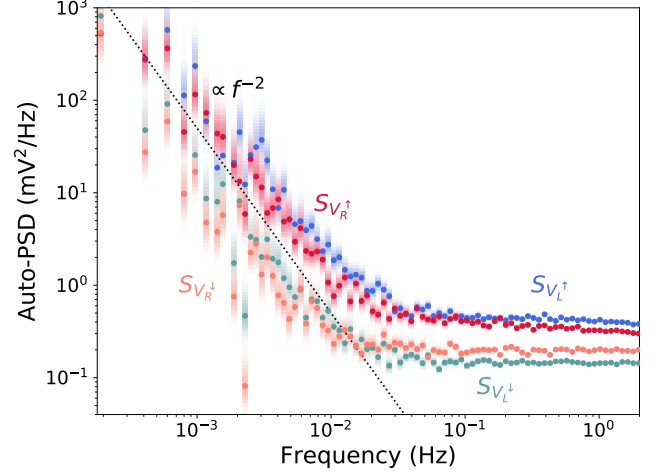

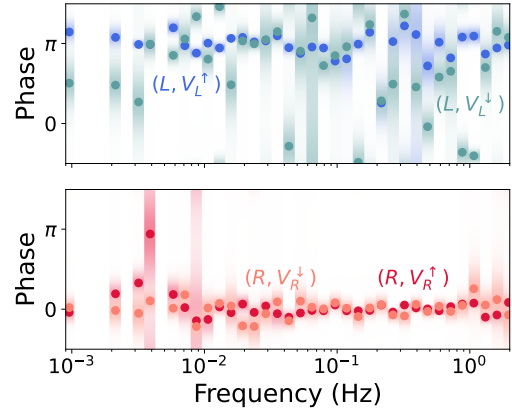FIG. 7. Auto-PSDs of the charge sensor voltages.

FIG. 8. Phase of the cross-PSDs between the charge sensor signals and the qubit energies.

Appendix B: PSDs of charge sensor signals

The charge sensor can be used to directly probe electric noise. Instead of acquiring separate data for the sensor, we average the voltages from the single-shot measurements that after binarization are used to estimate the qubit frequencies. These single-shot voltages correspond to the difference between the maximum and the minimum rf voltages acquired during the readout time window. If the single-shot readout voltage is above the threshold the spin outcome is determined as $|\uparrow\rangle$, otherwise as $|\downarrow\rangle$. We estimate a qubit frequency value from a single record composed of 100 single-shot measurements, then two sensor voltages are obtained by averaging the voltages that yield the same spin outcome out of those 100 values. Since the measurement stage is performed at two different operation points, as explained in the main text, we have a total of four sensor voltages V_α^σ, with $\alpha \in \{L, R\}$ and $\sigma \in \{\uparrow, \downarrow\}$, relating to which qubit is being measured and the spin readout result. The auto-PSDs of all charge sensor signals are
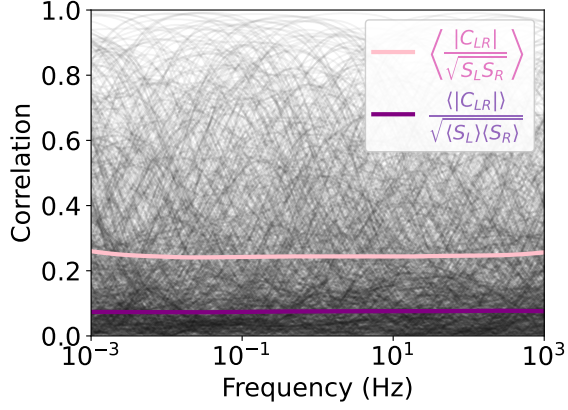
FIG. 9. Normalized cross-PSD amplitude calculated from an ensemble of 1000 sets of TLSs for 200 nm interqubit separation. The black lines correspond to the 1000 spectra of individual sets, and the ensemble average for $\langle r \rangle$ is plotted in pink and for $\bar{r}$ in purple.
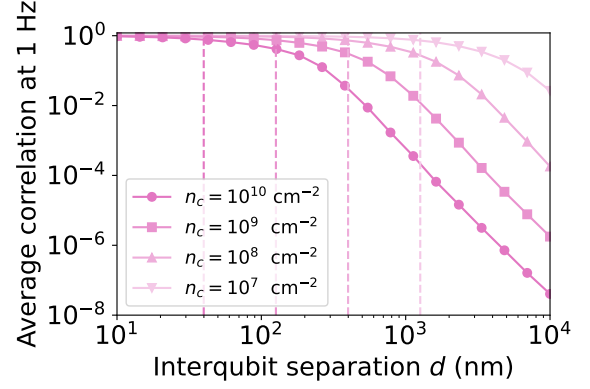

FIG. 10. Average normalized cross-PSD amplitude $\langle r \rangle$ at 1 Hz for different densities of TLSs. Vertical dashed lines give the mean distance between TLSs, equal to $1/\sqrt{2\pi n_c}$.

displayed in Fig. 7. There, we can observe a dependence $\propto f^{-2}$ in the low-frequency spectra similar to that seen in the qubits' noise spectra from Fig. 2a. This similarity may suggest a dominance of charge noise in qubit dephasing, but the conclusive evidence is found in the cross-PSDs between qubit energies and sensor voltages, which have their magnitudes displayed in Fig. 3 and their phases in Fig. 8. We find strong correlations with well defined phases and high confidence level, demonstrating our device is dominated by noise of an electric origin. Furthermore, the non-uniform character of these correlations with the charge sensor reinforces the idea that there is a non-uniform distribution of noise sources.

Appendix C: Scaling of cross-correlations with distance

When we simulate random ensembles of TLSs, the noise spectral characteristics vary for each distribution. Namely, the spectra are given by the properties of a few TLSs, making the results not self-averaging [76]. This is demonstrated in Fig. 9, which shows that the normalized cross-PSD can take basically any value between uncorrelated and perfectly correlated noise. On the other hand, the average (be it $\langle r \rangle$ or $\bar{r}$) takes on an almost constant value independent of frequency (any small features seen probably arise from our finite sampling). This allows us to extract a mean correlation strength for a certain interqubit separation. For convention, we take the value at 1 Hz but the scaling with distance is independent of this choice.

When the qubits are further apart, strong cross-correlations become less likely and the average $\langle r \rangle$ decreases. The interqubit separation at which correlations start to decay is determined by the mean distance between TLSs as is shown in Fig. 10. At higher densities, the TLSs are closer to each other such that it becomes

more probable for the two qubits to strongly couple to a different group of TLSs, leading to small noise cross-correlations. Although the average correlation magnitude decreases with increasing density of charge fluctuators, the overall noise amplitude increases proportionally.

Appendix D: Analytical calculation of $\bar{r}$

Here, we present an analytical calculation of $\bar{r} = \langle |C_{LR}| \rangle / \sqrt{\langle S_L \rangle \langle S_R \rangle}$ to determine the scaling of cross-correlations with the interqubit separation.

We start by treating each charge TLS with its image as an electric dipole, with fluctuating moment $\delta\vec{p} = \delta q\vec{l} = \delta q l \hat{y}$. Following the parameters of our device, the y coordinate of every TLS is $y_0 = -52$ nm, the effective ipole length is $l = 4$ nm, and the qubits are at $y = 0$. In this way, the x component of the electric field at the position $\vec{x}_\alpha$ of qubit α due to a single TLS-image pair k, located at $\vec{x}_k = (x_k, y_0, z_k)$, can be approximated as:

$$\delta E_{x,k}^{\text{dip}}(\vec{x}) \approx \delta q_k \frac{3y_0 l}{4\pi\epsilon\epsilon_0} \frac{x_\alpha - x_k}{[(x_\alpha - x_k)^2 + y_0^2 + z_k^2]^{5/2}}. \quad \text{(D1)}$$

With this, the correlator of electric fields is:

$$
\begin{aligned}
C_{E_\alpha^x E_\beta^x}(f) = \chi_0 \sum_{k=1}^{N_{\text{TLS}}} &\frac{(x_\alpha - x_k)}{[(x_\alpha - x_k)^2 + y_0^2 + z_k^2]^{5/2}} \\
&\times \frac{(x_\beta - x_k)}{[(x_\beta - x_k)^2 + y_0^2 + z_k^2]^{5/2}} \\
&\times \frac{t_k}{1 + 4\pi^2 t_k^2 f^2},
\end{aligned}
\quad \text{(D2)}
$$

with $\chi_0 \equiv \frac{9e^2}{2\epsilon^2} \frac{y_0^2 l^2}{(4\pi\epsilon_0)^2}$ and $\alpha, \beta \in \{L, R\}$. Upon averaging over TLS parameters, the summation over ensembles and over TLSs can be replaced by integrals with a corresponding probability distribution for those parameters. We assume a uniform probability distribution for
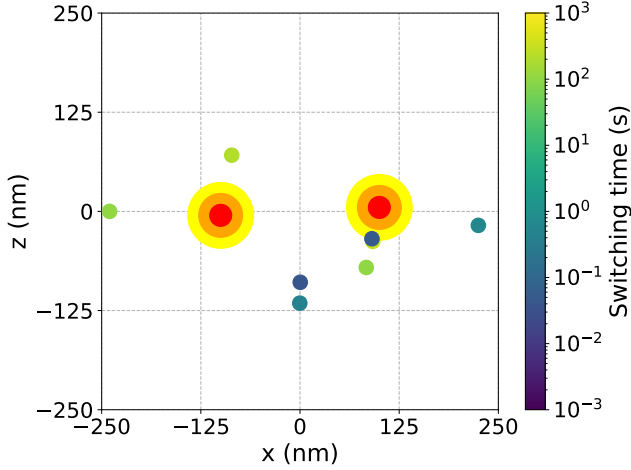
FIG. 11. Another set of TLSs that fits the measured data.

the position of the TLSs, equal to the density n_c, and a distribution $\rho(t)$ for the switching time. Then, the average for the correlator of electric fields is:

$$\langle C_{E_\alpha^x E_\beta^x}(f)\rangle = \chi_0 n_c \int_{-\infty}^{\infty} dx dz \frac{(x_\alpha - x)}{[(x_\alpha - x)^2 + y_0^2 + z^2]^{5/2}}$$
$$\times \frac{(x_\beta - x)}{[(x_\beta - x)^2 + y_0^2 + z^2]^{5/2}}$$
$$\times \int_0^{\infty} dt \, \rho(t) \frac{t}{1 + 4\pi^2 t^2 f^2}.$$

For the auto-correlations, the integral in space can be solved analytically, obtaining:

$$\langle S_{E_\alpha^x}(f)\rangle = \frac{\chi_0 n_c \pi}{24 y_0^6} G(f), \tag{D3}$$

where we defined $G(f) \equiv \int_0^{\infty} dt \, \rho(t) t/(1 + 4\pi^2 t^2 f^2)$. For the cross-correlation, we could evaluate the leading order in an expansion of the integrand in powers of y_0/d around $x = \pm d/2$. We obtained:

$$\langle |C_{E_L^x E_R^x}(f)|\rangle = \frac{\chi_0 n_c \pi}{192 y_0 d^5} G(f) + \mathcal{O}\left(d^{-7}\right). \tag{D4}$$

Equations (D3) and (D4) give:

$$\bar{r} = \frac{\langle |C_{LR}(f)|\rangle}{\sqrt{\langle S_L(f)\rangle \langle S_R(f)\rangle}} = \frac{1}{8} \frac{y_0^5}{d^5}, \tag{D5}$$

where the functions $G(f)$ cancel out making the result independent of the specific time distribution $\rho(t)$. This result is plotted as a purple line in Fig. 5.

Appendix E: Non-uniqueness of the distribution of fluctuators

The distribution of TLSs that can reproduce our results is not unique. Figure 11 depicts a different ensemble of fluctuators that also leads to a satisfactory fit of the data plotted in Fig. 2.

[1] M. Veldhorst, J. C. C. Hwang, C. H. Yang, A. W. Leenstra, B. de Ronde, J. P. Dehollain, J. T. Muhonen, F. E. Hudson, K. M. Itoh, A. Morello, and A. S. Dzurak, An addressable quantum dot qubit with fault-tolerant control-fidelity, Nat. Nanotechnol. **9**, 981 (2014).

[2] K. Takeda, J. Kamioka, T. Otsuka, J. Yoneda, T. Nakajima, M. R. Delbecq, S. Amaha, G. Allison, T. Kodera, S. Oda, and S. Tarucha, A fault-tolerant addressable spin qubit in a natural silicon quantum dot, Sci. Adv. **2**, e1600694 (2016).

[3] T. Nakajima, M. R. Delbecq, T. Otsuka, P. Stano, S. Amaha, J. Yoneda, A. Noiri, K. Kawasaki, K. Takeda, G. Allison, A. Ludwig, A. D. Wieck, D. Loss, and S. Tarucha, Robust single-shot spin measurement with 99.5% fidelity in a quantum dot array, Phys. Rev. Lett. **119**, 017701 (2017).

[4] T. F. Watson, S. G. J. Philips, E. Kawakami, D. R. Ward, P. Scarlino, M. Veldhorst, D. E. Savage, M. G. Lagally, M. Friesen, S. N. Coppersmith, M. A. Eriksson, and L. M. K. Vandersypen, A programmable two-qubit quantum processor in silicon, Nature **555**, 633 (2018).

[5] D. M. Zajac, A. J. Sigillito, M. Russ, F. Borjans, J. M. Taylor, G. Burkard, and J. R. Petta, Resonantly driven cnot gate for electron spins, Science **359**, 439 (2018).

[6] K. Takeda, J. Yoneda, T. Otsuka, T. Nakajima, M. R. Delbecq, G. Allison, Y. Hoshi, N. Usami, K. M. Itoh, S. Oda, T. Kodera, and S. Tarucha, Optimized electrical control of a Si/SiGe spin qubit in the presence of an induced frequency shift, npj Quantum Inf. **4**, 54 (2018).

[7] J. Yoneda, K. Takeda, T. Otsuka, T. Nakajima, M. R. Delbecq, G. Allison, T. Honda, T. Kodera, S. Oda, Y. Hoshi, N. Usami, K. M. Itoh, and S. Tarucha, A quantum-dot spin qubit with coherence limited by charge noise and fidelity higher than 99.9%, Nat. Nanotechnol. **13**, 102 (2018).

[8] X. Xue, T. F. Watson, J. Helsen, D. R. Ward, D. E. Savage, M. G. Lagally, S. N. Coppersmith, M. A. Eriksson, S. Wehner, and L. M. K. Vandersypen, Benchmarking gate fidelities in a Si/SiGe two-qubit device, Phys. Rev. X **9**, 021011 (2019).

[9] T. Nakajima, A. Noiri, J. Yoneda, M. R. Delbecq, P. Stano, T. Otsuka, K. Takeda, S. Amaha, G. Allison, K. Kawasaki, A. Ludwig, A. D. Wieck, D. Loss, and S. Tarucha, Quantum non-demolition measurement of an electron spin qubit, Nat. Nanotechnol. **14**, 555 (2019).

[10] C. H. Yang, K. W. Chan, R. Harper, W. Huang, T. Evans, J. C. C. Hwang, B. Hensen, A. Laucht, T. Tanttu, F. E. Hudson, S. T. Flammia, K. M. Itoh, A. Morello, S. D. Bartlett, and A. S. Dzurak, Silicon qubit fidelities approaching incoherent noise limits via pulse engineering, Nat. Electron. **2**, 151 (2019).

[11] K. Takeda, A. Noiri, J. Yoneda, T. Nakajima, and S. Tarucha, Resonantly driven singlet-triplet spin qubit in silicon, Phys. Rev. Lett. **124**, 117701 (2020).

[12] J. Yoneda, K. Takeda, A. Noiri, T. Nakajima, S. Li, J. Kamioka, T. Kodera, and S. Tarucha, Quantum nondemolition readout of an electron spin in silicon, Nat. Commun. **11**, 1144 (2020).

[13] A. Noiri, K. Takeda, J. Yoneda, T. Nakajima, T. Kodera, and S. Tarucha, Radio-frequency-detected fast charge sensing in undoped silicon quantum dots, Nano Lett. **20**, 947 (2020).

[14] J. Z. Blumoff, A. S. Pan, T. E. Keating, R. W. Andrews, D. W. Barnes, T. L. Brecht, E. T. Croke, L. E. Euliss, J. A. Fast, C. A. C. Jackson, A. M. Jones, J. Kerckhoff, R. K. Lanza, K. Raach, B. J. Thomas, R. Velunta, A. J. Weinstein, T. D. Ladd, K. Eng, M. G. Borselli, A. T. Hunter, and M. T. Rakher, Fast and high-fidelity state preparation and measurement in triple-quantum-dot spin qubits, PRX Quantum **3**, 010352 (2022).

[15] X. Xue, M. Russ, N. Samkharadze, B. Undseth, A. Sammak, G. Scappucci, and L. M. K. Vandersypen, Quantum logic with spin qubits crossing the surface code threshold, Nature **601**, 343 (2022).

[16] A. R. Mills, C. R. Guinn, M. J. Gullans, A. J. Sigillito, M. M. Feldman, E. Nielsen, and J. R. Petta, Two-qubit silicon quantum processor with operation fidelity exceeding 99%, Sci. Adv. **8**, eabn5130 (2022).

[17] A. R. Mills, C. R. Guinn, M. M. Feldman, A. J. Sigillito, M. J. Gullans, M. T. Rakher, J. Kerckhoff, C. A. C. Jackson, and J. R. Petta, High-fidelity state preparation, quantum control, and readout of an isotopically enriched silicon spin qubit, Phys. Rev. Appl. **18**, 064028 (2022).

[18] A. Noiri, K. Takeda, T. Nakajima, T. Kobayashi, A. Sammak, G. Scappucci, and S. Tarucha, Fast universal quantum gate above the fault-tolerance threshold in silicon, Nature **601**, 338 (2022).

[19] J. Preskill, Sufficient condition on noise correlations for scalable quantum computing, Quantum Inf. Comput. **13**, 181–194 (2013).

[20] D. Aharonov, A. Kitaev, and J. Preskill, Fault-tolerant quantum computation with long-range correlated noise, Phys. Rev. Lett. **96**, 050504 (2006).

[21] J. P. Clemens, S. Siddiqui, and J. Gea-Banacloche, Quantum error correction against correlated noise, Phys. Rev. A **69**, 062313 (2004).

[22] P. Szańkowski, M. Trippenbach, and L. Cywiński, Spectroscopy of cross correlations of environmental noises with two qubits, Phys. Rev. A **94**, 012109 (2016).

[23] G. A. Paz-Silva, L. M. Norris, and L. Viola, Multiqubit spectroscopy of gaussian quantum noise, Phys. Rev. A **95**, 022121 (2017).

[24] V. N. Premakumar and R. Joynt, Error mitigation in quantum computers subject to spatially correlated noise, arXiv:1812.07076.

[25] J. M. Boter, X. Xue, T. Krähenmann, T. F. Watson, V. N. Premakumar, D. R. Ward, D. E. Savage, M. G. Lagally, M. Friesen, S. N. Coppersmith, M. A. Eriksson, R. Joynt, and L. M. K. Vandersypen, Spatial noise correlations in a Si/SiGe two-qubit device from bell state coherences, Phys. Rev. B **101**, 235133 (2020).

[26] U. von Lüpke, F. Beaudoin, L. M. Norris, Y. Sung, R. Winik, J. Y. Qiu, M. Kjaergaard, D. Kim, J. Yoder, S. Gustavsson, L. Viola, and W. D. Oliver, Two-qubit spectroscopy of spatiotemporally correlated quantum noise in superconducting qubits, PRX Quantum **1**, 010305 (2020).

[27] J. Yoneda, J. S. Rojas-Arias, P. Stano, K. Takeda, A. Noiri, T. Nakajima, D. Loss, and S. Tarucha, Noise-correlation spectrum for a pair of spin qubits in silicon, Nature Physics 10.1038/s41567-023-02238-6 (2023).

[28] D. Loss and D. P. DiVincenzo, Quantum computation with quantum dots, Phys. Rev. A **57**, 120 (1998).

[29] R. Hanson, L. P. Kouwenhoven, J. R. Petta, S. Tarucha, and L. M. K. Vandersypen, Spins in few-electron quantum dots, Rev. Mod. Phys. **79**, 1217 (2007).

[30] D. J. Reilly, J. M. Taylor, E. A. Laird, J. R. Petta, C. M. Marcus, M. P. Hanson, and A. C. Gossard, Measurement of temporal correlations of the overhauser field in a double quantum dot, Phys. Rev. Lett. **101**, 236803 (2008).

[31] F. K. Malinowski, F. Martins, L. Cywiński, M. S. Rudner, P. D. Nissen, S. Fallahi, G. C. Gardner, M. J. Manfra, C. M. Marcus, and F. Kuemmeth, Spectrum of the nuclear environment for GaAs spin qubits, Phys. Rev. Lett. **118**, 177702 (2017).

[32] S. Tenberg, R. P. G. McNeil, S. Rubbert, and H. Bluhm, Narrowing of the overhauser field distribution by feedback-enhanced dynamic nuclear polarization, Phys. Rev. B **92**, 195428 (2015).

[33] E. A. Chekhovich, M. N. Makhonin, A. I. Tartakovskii, A. Yacoby, H. Bluhm, K. C. Nowack, and L. M. K. Vandersypen, Nuclear spin effects in semiconductor quantum dots, Nat. Mater. **12**, 494 (2013).

[34] F. A. Zwanenburg, A. S. Dzurak, A. Morello, M. Y. Simmons, L. C. L. Hollenberg, G. Klimeck, S. Rogge, S. N. Coppersmith, and M. A. Eriksson, Silicon quantum electronics, Rev. Mod. Phys. **85**, 961 (2013).

[35] E. J. Connors, J. J. Nelson, H. Qiao, L. F. Edge, and J. M. Nichol, Low-frequency charge noise in Si/SiGe quantum dots, Phys. Rev. B **100**, 165305 (2019).

[36] B. M. Freeman, J. S. Schoenfield, and H. Jiang, Comparison of low frequency charge noise in identically patterned Si/SiO2 and Si/SiGe quantum dots, Appl. Phys. Lett. **108**, 253108 (2016).

[37] T. Struck, A. Hollmann, F. Schauer, O. Fedorets, A. Schmidbauer, K. Sawano, H. Riemann, N. V. Abrosimov, Ł. Cywiński, D. Bougeard, and L. R. Schreiber, Low-frequency spin qubit energy splitting noise in highly purified ^{28}Si/SiGe, npj Quantum Inf. **6**, 40 (2020).

[38] A. Wild, J. Kierig, J. Sailer, J. W. Ager, E. E. Haller, G. Abstreiter, S. Ludwig, and D. Bougeard, Few electron double quantum dot in an isotopically purified ^{28}Si quantum well, Appl. Phys. Lett. **100**, 143110 (2012).

[39] J. P. Dehollain, J. T. Muhonen, R. Blume-Kohout, K. M. Rudinger, J. K. Gamble, E. Nielsen, A. Laucht, S. Simmons, R. Kalra, A. S. Dzurak, and A. Morello, Optimization of a solid-state electron spin qubit using gate set tomography, New J. Phys. **18**, 103018 (2016).

[40] P. Harvey-Collard, N. T. Jacobson, C. Bureau-Oxton, R. M. Jock, V. Srinivasa, A. M. Mounce, D. R. Ward, J. M. Anderson, R. P. Manginell, J. R. Wendt, T. Pluym, M. P. Lilly, D. R. Luhman, M. Pioro-Ladrière, and M. S. Carroll, Spin-orbit interactions for singlet-triplet qubits in silicon, Phys. Rev. Lett. **122**, 217702 (2019).

[41] R. Zhao, T. Tanttu, K. Y. Tan, B. Hensen, K. W. Chan, J. C. C. Hwang, R. C. C. Leon, C. H. Yang, W. Gilbert, F. E. Hudson, K. M. Itoh, A. A. Kiselev, T. D. Ladd, A. Morello, A. Laucht, and A. S. Dzurak, Single-spin qubits in isotopically enriched silicon at low magnetic field, Nat. Commun. **10**, 5500 (2019).

[42] B. Hensen, W. Wei Huang, C.-H. Yang, K. Wai Chan, J. Yoneda, T. Tanttu, F. E. Hudson, A. Laucht, K. M. Itoh, T. D. Ladd, A. Morello, and A. S. Dzurak, A silicon quantum-dot-coupled nuclear spin qubit, Nat. Nanotechnol. **15**, 13 (2020).

[43] F. Hooge, 1/f noise, Physica B+C **83**, 14 (1976).

[44] M. Pioro-Ladrière, T. Obata, Y. Tokura, Y.-S. Shin, T. Kubo, K. Yoshida, T. Taniyama, and S. Tarucha, Electrically driven single-electron spin resonance in a slanting zeeman field, Nat. Phys. **4**, 776 (2008).

[45] J. Yoneda, T. Otsuka, T. Takakura, M. Pioro-Ladrière, R. Brunner, H. Lu, T. Nakajima, T. Obata, A. Noiri, C. J. Palmstrøm, A. C. Gossard, and S. Tarucha, Robust micromagnet design for fast electrical manipulations of single spins in quantum dots, Appl. Phys. Express **8**, 084401 (2015).

[46] A. Kha, R. Joynt, and D. Culcer, Do micromagnets expose spin qubits to charge and Johnson noise?, Appl. Phys. Lett. **107**, 172101 (2015).

[47] By a $1/f$-like spectrum we mean a spectrum proportional to $1/f^\alpha$ with $0 < \alpha < 2$.

[48] Sh. Kogan, *Electronic Noise and Fluctuations in Solids*, 1st ed. (Cambridge University Press, 1996).

[49] D. J. Reilly, J. M. Taylor, E. A. Laird, J. R. Petta, C. M. Marcus, M. P. Hanson, and A. C. Gossard, Measurement of Temporal Correlations of the Overhauser Field in a Double Quantum Dot, Physical Review Letters **101**, 236803 (2008).

[50] F. K. Malinowski, F. Martins, Ł. Cywiński, M. S. Rudner, P. D. Nissen, S. Fallahi, G. C. Gardner, M. J. Manfra, C. M. Marcus, and F. Kuemmeth, Spectrum of the Nuclear Environment for GaAs Spin Qubits, Physical Review Letters **118**, 177702 (2017).

[51] R. M. Jock, N. T. Jacobson, M. Rudolph, D. R. Ward, M. S. Carroll, and D. R. Luhman, A silicon singlet–triplet qubit driven by spin-valley coupling, Nat. Commun. **13**, 641 (2022).

[52] A. Elsayed, M. Shehata, C. Godfrin, S. Kubicek, S. Massar, Y. Canvel, J. Jussot, G. Simion, M. Mongillo, D. Wan, B. Govoreanu, I. P. Radu, R. Li, P. Van Dorpe, and K. De Greve, Low charge noise quantum dots with industrial CMOS manufacturing (2022), arXiv:2212.06464.

[53] E. J. Connors, J. Nelson, L. F. Edge, and J. M. Nichol, Charge-noise spectroscopy of Si/SiGe quantum dots via dynamically-decoupled exchange oscillations, Nat. Commun. **13**, 940 (2022).

[54] H. Wong, Low-frequency noise study in electron devices: Review and update, Microelectronics Reliability **43**, 585 (2003).

[55] C. Müller, J. H. Cole, and J. Lisenfeld, Towards understanding two-level-systems in amorphous solids – Insights from quantum circuits, Reports on Progress in Physics **82**, 124501 (2019), arxiv:1705.01108 [cond-mat, physics:quant-ph].

[56] M. R. Delbecq, T. Nakajima, P. Stano, T. Otsuka, S. Amaha, J. Yoneda, K. Takeda, G. Allison, A. Ludwig, A. D. Wieck, and S. Tarucha, Quantum dephasing in a gated GaAs triple quantum dot due to nonergodic noise, Phys. Rev. Lett. **116**, 046802 (2016).

[57] T. Nakajima, A. Noiri, K. Kawasaki, J. Yoneda, P. Stano, S. Amaha, T. Otsuka, K. Takeda, M. R. Delbecq, G. Allison, A. Ludwig, A. D. Wieck, D. Loss, and S. Tarucha, Coherence of a driven electron spin qubit actively decoupled from quasistatic noise, Phys. Rev. X **10**, 011060 (2020).

[58] D. M. Zajac, T. M. Hazard, X. Mi, K. Wang, and J. R. Petta, A reconfigurable gate architecture for Si/SiGe quantum dots, Appl. Phys. Lett. **106**, 223507 (2015).

[59] J. M. Elzerman, R. Hanson, L. H. Willems van Beveren, B. Witkamp, L. M. K. Vandersypen, and L. P. Kouwenhoven, Single-shot read-out of an individual electron spin in a quantum dot, Nature **430**, 431 (2004).

[60] A. Noiri, K. Takeda, T. Nakajima, T. Kobayashi, A. Sammak, G. Scappucci, and S. Tarucha, A shuttling-based two-qubit logic gate for linking distant silicon quantum processors, Nat. Commun. **13**, 5740 (2022).

[61] A. Gutiérrez-Rubio, J. S. Rojas-Arias, J. Yoneda, S. Tarucha, D. Loss, and P. Stano, Bayesian estimation of correlation functions, Phys. Rev. Res. **4**, 043166 (2022).

[62] S. Machlup, Noise in semiconductors: Spectrum of a two-parameter random signal, J. Appl. Phys. **25**, 341 (1954).

[63] This example highlights the importance of providing a level of confidence when reporting noise spectra and is the reason why we use the Bayesian estimation of correlation functions from Ref. [61].

[64] A. McWhorter and L. Laboratory, *1/f Noise and Related Surface Effects in Germanium*, Technical report (Lincoln Laboratory) (Massachusetts Institute of Technology, Department of Electrical Engineering, 1955).

[65] Based on the way how the sensor signals are processed, we expect cross-correlations to occur only for $V_\alpha^\uparrow$. We believe that the finite correlations of $V_\alpha^\downarrow$ (visible also in Fig. 7 as a low frequency tail) arise from wrong assignments of the up-down label due to using the usual threshold-voltage method.

[66] J. Bernamont, Fluctuations de potentiel aux bornes d'un conducteur métallique de faible volume parcouru par un courant, Annales de physique **11**, 71 (1937).

[67] S. Machlup, Noise in Semiconductors: Spectrum of a Two-Parameter Random Signal, Journal of Applied Physics **25**, 341 (1954).

[68] A. L. McWhorter, *1/f Noise and Related Surface Effects in Germanium*, Ph.D. thesis, MIT, Cambridge, Massachusetts (1955).

[69] P. Dutta and P. M. Horn, Low-frequency fluctuations in solids: 1 f noise, Reviews of Modern Physics **53**, 497 (1981).

[70] F. Hooge, 1/f noise sources, IEEE Transactions on Electron Devices **41**, 1926 (Nov./1994).

[71] A. V. Kuhlmann, J. Houel, A. Ludwig, L. Greuter, D. Reuter, A. D. Wieck, M. Poggio, and R. J. Warburton, Charge noise and spin noise in a semiconductor quantum device, Nat. Phys. **9**, 570 (2013).

[72] D. M. Zajac, T. M. Hazard, X. Mi, E. Nielsen, and J. R. Petta, Scalable gate architecture for a one-dimensional array of semiconductor spin qubits, Phys. Rev. Applied **6**, 054013 (2016).

[73] M. B. Weissman, $\frac{1}{f}$ noise and other slow, nonexponential kinetics in condensed matter, Rev. Mod. Phys. **60**,

537 (1988).

[74] M. M. E. K. Shehata, G. Simion, R. Li, F. A. Mohiyaddin, D. Wan, M. Mongillo, B. Govoreanu, I. Radu, K. De Greve, and P. Van Dorpe, Modelling semiconductor spin qubits and their charge noise environment for quantum gate fidelity estimation (2022), arxiv:2210.04539 [cond-mat, physics:quant-ph].

[75] We note that since the space and time coordinates in the correlators factorize, the ensemble-averaged normalized cross-PSD, and thus the scaling of the cross-correlations with distance, is independent of the specific distribution of switching times; see Eq. (D5) and the comment beneath it.

[76] J. Schriefl, Y. Makhlin, A. Shnirman, and G. Schön, Decoherence from ensembles of two-level fluctuators, New J. Phys. **8**, 1 (2006).

[77] As an example, Ref. [20] concludes that correlations should decay faster than d^{-2} in two-dimensional arrays.

[78] B. P. Wuetz, D. D. Esposti, A. M. J. Zwerver, S. V. Amitonov, M. Botifoll, J. Arbiol, A. Sammak, L. M. K. Vandersypen, M. Russ, and G. Scappucci, Reducing charge noise in quantum dots by using thin silicon quantum wells, arXiv:2209.07242.

[79] J. M. Taylor, *Hyperfine interactions and quantum information processing in quantum dots*, Ph.D. thesis, Harvard University (2006).

[80] P. Philippopoulos, S. Chesi, and W. A. Coish, First-principles hyperfine tensors for electrons and holes in gaas and silicon, Phys. Rev. B **101**, 115302 (2020).

[81] L. V. C. Assali, H. M. Petrilli, R. B. Capaz, B. Koiller, X. Hu, and S. Das Sarma, Hyperfine interactions in silicon quantum dots, Phys. Rev. B **83**, 165301 (2011).

[82] J. Schliemann, A. Khaetskii, and D. Loss, Electron spin dynamics in quantum dots and related nanostructures due to hyperfine interaction with nuclei, J. Phys. Condens. Matter **15**, R1809 (2003).

[83] H. Hayashi, K. M. Itoh, and L. S. Vlasenko, Nuclear magnetic resonance linewidth and spin diffusion in ^{29}Si isotopically controlled silicon, Phys. Rev. B **78**, 153201 (2008).